Sensors and Actuators Reports 5 (2023) 100161

Contents lists available at ScienceDirect

Sensors and Actuators Reports

journal homepage: www.sciencedirect.com/journal/sensors-and-actuators-reports

Wearable graphene-based fabric electrodes for enhanced and long-term biosignal detection

Babar Ali [a,b,*], Hossein Cheraghi Bidsorkhi [a,b], Alessandro G. D'Aloia [a,b], Marco Laracca [a], Maria S. Sarto [a,b]

[a] Dept. of Astronautical Electrical and Energy Engineering, Sapienza University of Rome, Italy
[b] Research Center for Nanotechnology applied to Engineering (CNIS), Rome, Italy

ARTICLE INFO

Keywords:
Wearable
Graphene
Biosignal electrode
Electrocardiograph
ECG signal features
Skin-electrode contact
Real-time monitoring

ABSTRACT

Wearable health sensing devices are crucial and the development of multi-sensing textiles for non-invasive and continuous long-term biosignal monitoring is of primary interest. Nowadays, different wearable sensors are available but they usually lack comfort for continuous use during normal daily life activities. In this study, new graphene-based flexible dry electrodes are investigated to overcome the limitations of the currently available electrodes. Briefly, they are realized through casting PVDF (polyvinylidene fluoride)/GNP (graphene nanoplatelets) nanocomposite over commercial textiles. These electrodes are soft and flexible and adhere more easily to the skin. In terms of performance, the PVDF/GNP electrodes show lower impedance per unit area compared to commercial ones, hence they can be employed for biosignal detection. In particular, the developed electrodes are used for electrocardiogram (ECG) signal monitoring. The recorded ECG signal-to-noise ratio (SNR) reached up to 40 dB and all necessary ECG signal features and intervals are clearly distinguishable. Furthermore, the essential ECG signal intervals on each cadiac cycle show very small variations in time. Finally, the superhydrophobic property allows the electrodes to be used repeatedly after washing. As a final note, the developed dry PVDF/GNP electrodes provide reusability, biocompatibility, good skin-electrode contact, and no signs of skin irritation.

1. Introduction

Cardiovascular diseases (CVDs) are one of the major reasons of death globally: every year an estimated 32% of people die due to heart-related diseases [1]. Therefore, continuous and real-time monitoring of heart activity of patients with chronic CVDs would enable the recognition of symptoms and alerts for such diseases. However, the growing healthcare cost due to population aging made it very difficult to provide observations of chronic diseases over long periods. It is a challenge for engineers and doctors to develop improved monitoring technology, superior to available methods in terms of cost-effectiveness, reliability, and portability. Thankfully, the recent progress in wearable technology and telecommunication made it practical to monitor health conditions remotely, regardless of a patient's activity and location [2–6].

One of the most common ways of noninvasive diagnosis of arrhythmia, hypertension, and other heart-related abnormalities is the Electrocardiogram (ECG), i-e., the electrical activity of the heart plotted in a voltage versus time graph [7,8]. Generally, a noninvasive method of acquiring ECG is performed by placing two or more biopotential electrodes on the surface of the skin (usually on the chest) of the subject. Typically, gelled silver/silver chloride (Ag/AgCl) electrodes are used for recording biopotential signals like ECG, electroencephalogram (EEG), electromyogram (EMG), etc. The gelled Ag/AgCl electrodes contain conductive Potassium chloride (KCl) electrolyte that performs the transduction of ion current to electron current into the circuit and has very low skin-electrodes impedance [9]. Nevertheless, long-term use of conductive gel on the skin undergoes significant drawbacks as it dries out over time, thus increasing the skin-electrode impedance [10]. This fact has a significant disadvantage on the quality of the recorded signal as it results in a poor signal-to-noise ratio (SNR). In addition, the extended use of gelled electrodes generally causes skin irritation and itchiness [11].

Over the past years, research in the development of dry biopotential electrodes has shown favorable results and could be used for a reliable measurement of biopotential signals, as a replacement for gelled electrodes. Dry electrodes construct a completely different interface with the

* Corresponding author.
E-mail address: babar.ali@uniroma1.it (B. Ali).

https://doi.org/10.1016/j.snr.2023.100161
Received 6 February 2023; Received in revised form 12 May 2023; Accepted 17 May 2023
Available online 23 May 2023

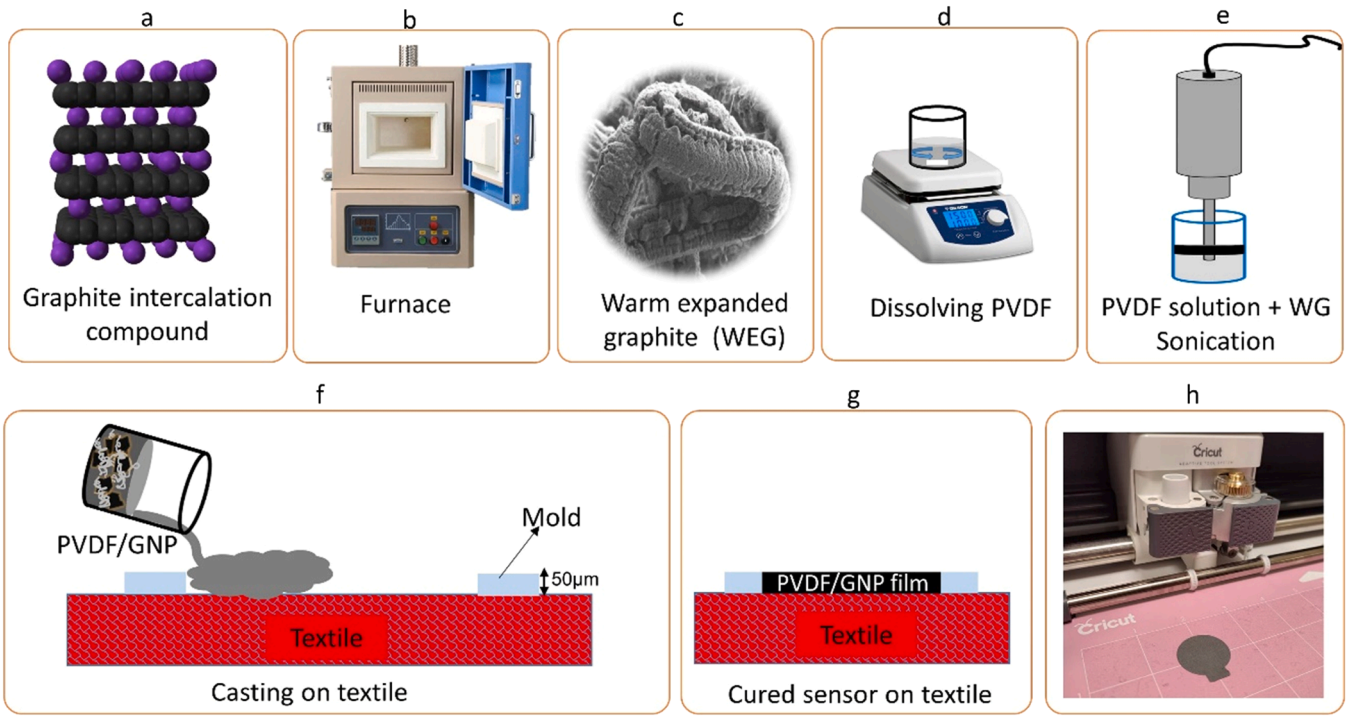

Fig. 1. (a) commercial graphite intercalation compound (GIC) (b) GIC expansion via high-temperature thermal shock method; (c) warm expanded graphite (d): dissolving PVDF (e) ultrasonic processor (f): coating mold on textile (g) curing sensor on textile (h) electrode shaping using Cricut®.

skin than gelled ones, thereby, being categorized as polarized and non-polarized electrodes. The first ones are characterized by charge separation between the electrode-electrolyte interface, hence, they have an absence of direct current hereby often called capacitive electrodes [12]. Whereas, non-polarized electrodes have no ideal separation of charges, hence, they have a direct current flow between the interface hereby they are often called conductive electrodes. Research in the past has shown certain advantages of conductive electrodes over capacitive ones in long-term wearable applications because the latter electrodes are highly sensitive to motion artifacts since charge distribution between electrode-skin interface changes notably under motion [13]. Moreover, polarized electrodes generally experience higher attenuation in low frequencies which results in low SNR and baseline fluctuations in biopotential measurement [14]. Also in polarized electrodes, the reduction of high skin-electrode impedance requires large electrode dimensions which makes it incompatible with wearable applications.

Many different dry conductive electrodes have been presented recently [15–17]. For instance, Zahed et al. [15] investigated flexible dry electrodes using a biocompatible polymer polyethylene-dioxythiophene: polystyrene-sulfonate (PEDOT: PSS) spray-coated on laser-induced graphene (LIG) of 10 mm diameter electrode. Chlaihawia et al. [16] developed dry electrodes by printing silver flake ink over polyethylene terephthalate substrate and later deposited multi-walled carbon nanotube/polydimethylsiloxane (MWCNT/PDMS) composite using bar coating, as conductive polymer. Yokus et al. [17] designed flexible dry electrodes by screen printing Ag/AgCl conductive ink on Vista-Maxx propylene-based elastomeric meltblown flexible nonwoven fabric in three different sizes 10, 20, and 30 mm diameter.

All these dry electrodes, although very effective, require an extensive manufacturing process and result in relatively higher impedance compared to frequently used commercial Ag/AgCl electrodes. Furthermore, the electrodes presented in the aforementioned papers are prepared on relatively rigid substrates and thus prone to motion artifacts. In addition, it is harder to place rigid electrodes on certain positions of the body due to their lack of flexibility resulting in a variation of the skin-electrode contact area and in some cases skin irritation along with itchiness [18].

Based on the above-mentioned considerations, the use of fabrics as substrates would provide better skin-electrode contact and comfort especially when long monitoring periods are required. Thus, the use of electrodes over fabrics overcomes the downsides of the electrodes discussed earlier. A good deal of textile fabrics woven, non-woven and yarns, either using conductive material or non-conductive materials coated with conductive polymers, have been studied to be used as biopotential electrodes [19–21]. These studies showed the possibility of using textile fabrics as ECG electrodes in wearable applications with several advantages in terms of flexibility, reusability, and washability.

In this work, flexible graphene coated fabrics working as dry biopotential electrodes are investigated. Briefly, they are realized through casting graphene based nanocomposites over commercial textiles. Graphene-based nanostructures are selected here as nanofillers due to their electrical and mechanical properties [22]. Their electromobility [23], thermal conductivity [24], and young's modulus [25] make graphene-based nanocomposites suitable for wearable, flexible, and high-sensitive transducers for electrical and optical applications [26, 27]. Therefore, graphene nanoplatelets (GNPs), short stacks of graphene sheets with an overall thickness of around ten nanometers, are mixed with polyvinylidene fluoride (PVDF) as the polymer matrix and coated over a fabric. The PVDF fluoropolymer has high resistance against solvents, a low density of 1.68 g/cm3 [28] and leads the coating to be superhydrophobic [29]. Hence, allowing the coated fabric to be washed repeatedly without losing its properties, and stand effective in situations like skin perspiration when used as biopotential electrodes [30,31]. Additionally, the preparation of this composite is straightforward and cheap leading them to be desirable for large-scale production.

Here, PVDF/GNP composites are cast over a commercial fabric with two different GNP concentrations and shaped into biopotential electrodes to record ECG signals through in vivo experimentation. At first, the produced electrodes are electrically characterized in terms of electrical conductivity and sheet resistance. Then, the graphene coating morphology is assessed via scanning electron microscopy (SEM). In addition, to get a preliminary indicator of their resistance to washing

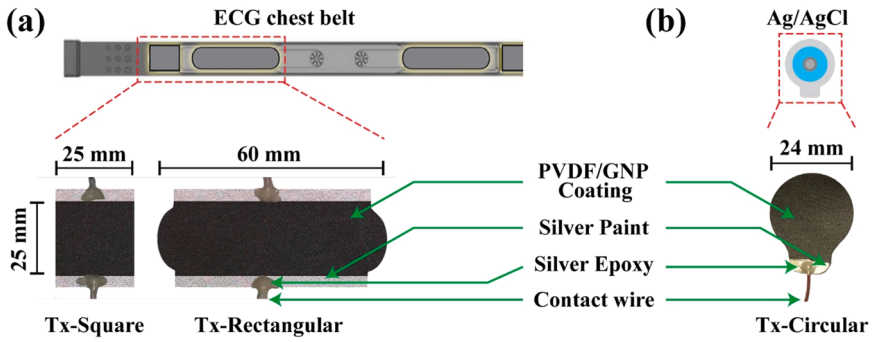

Fig. 2. (a) Electrodes in ECG chest belt taken as reference for square-shaped and rectangular-shaped PVDF/GNP electrodes (b) Disposable Ag/AgCl electrodes taken as reference for circular-shaped PVDF/GNP electrodes.

Table 1
PVDF/GNP coated samples dimensions and contact area.

Graphene coated fabric electrodes	Dimensions [mm]			Contact Area [mm^2]
	Length	Width	Diameter	
T1-Circular T2-Circular	–	–	24 mm	4.52
T1-Square T2-Square	25 mm	25 mm	–	5.75
T1-Rectangular T2- Rectangular	60 mm	25 mm	–	15.71

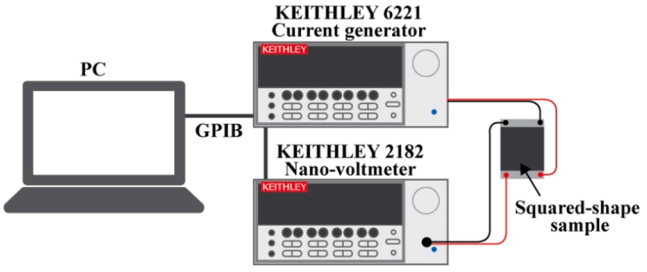

Fig. 3. Sheet resistance measurement setup using four-wire probe method.

cycles, the wettability of the coated textiles is assessed through water contact angle (CA) measurements. Moreover, GNPs possess characteristics that make them effective in filtering airborne pathogens, due to their antimicrobial and antiviral properties. Later, the skin-electrode impedance spectrum is measured by placing a pair of electrodes on the wrist. Finally, the ECG signals are measured by attaching one or more pairs of electrodes to an elastic belt strapped around the chest of the test subject. The ECG measurement results of each electrode are compared to the commercial wet Ag/AgCl and dry ECG best electrodes in terms of ECG signal features, ECG key interval variations, and SNR.

2. Materials and methods

2.1. Material preparation

At first, warm expanded graphite (WEG) is obtained through high-temperature thermal expansion of graphite intercalation compound (GIC), as described in [32]. The PVDF is then dissolved in an appropriate solvent at 65 °C by stirring the mixture with a magnetic stirrer. Using an ultrasonic processor, WEG is incorporated into the PVDF solution. Thus, a homogeneous suspension of GNPs is obtained in a solution of PVDF-Dimethylformamide (DMF) [33]. The GNP weight concentration with respect to the PVDF amount is 10% wt. and 13% wt. The PVDF/GNP mixture is subsequently cast onto a commercial polyester textile and quickly heated in an oven, as summarized in Fig. 1.

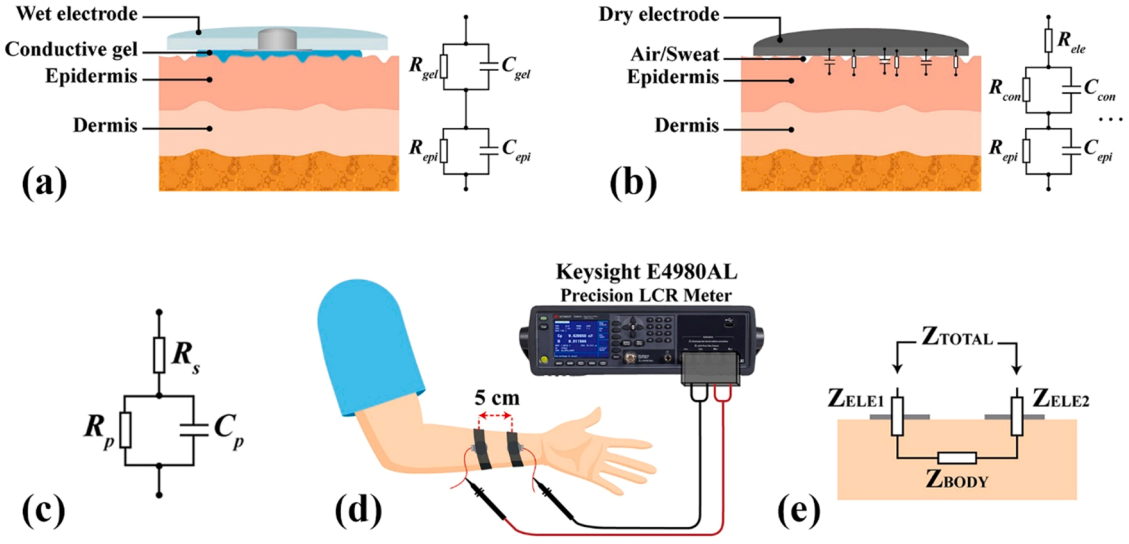

Fig. 4. (a) Skin-electrode interface and electrical equivalent circuit of wet Ag/AgCl electrode (b) skin-electrode interface and electrical equivalent circuit of dry PVDF/GNP flexible electrode (c) simplified first order RC equivalent time-constant model of skin (d) skin-electrode impedance measurement setup consisting of two electrodes attached to the inner forearm using elastic Velcro straps and an LCR meter (e) total impedance using a two-electrode impedance measurement scheme.

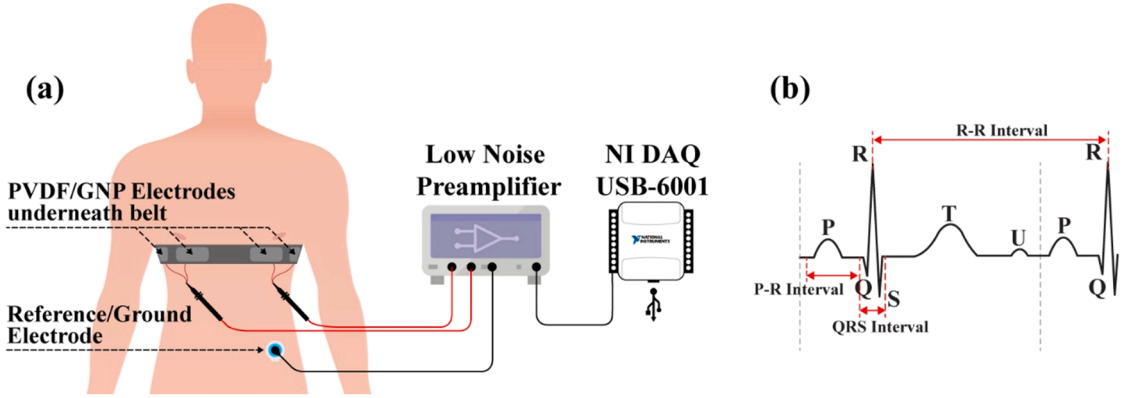

Fig. 5. (a) ECG measurement setup using pair of electrodes placed on the chest held steady with an elastic strap along with signal recording instruments (b) Illustration of normal ECG signal sinus rhythm and each segment labeled separately.

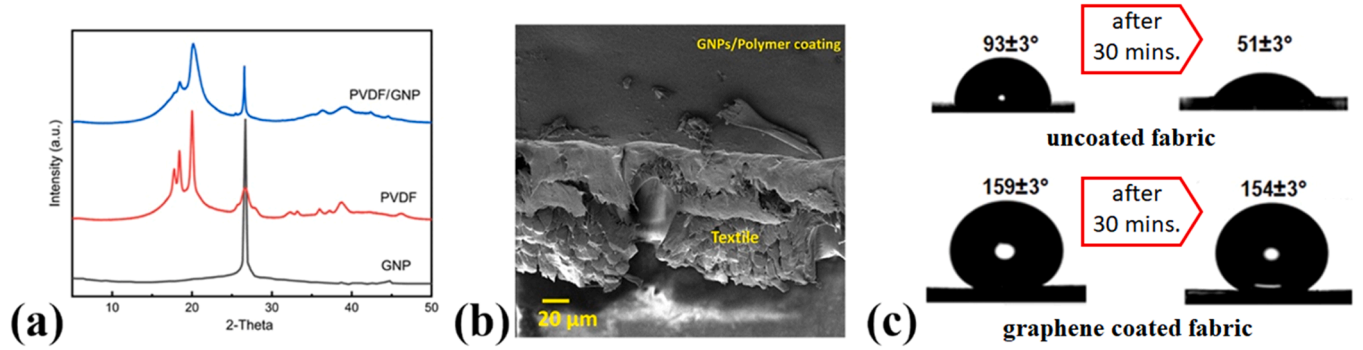

Fig. 6. (a) XRPD spectra of GNPs, PVDF coating and PVDF/GNP coating filled at 13% wt. (b) SEM image: surface of graphene coated textile (c) Contact angle measurements performed on uncoated and PVDF/GNP coated fabrics, performed during water droplet release and after 30 min.

Table 2
GNP concentrations, thicknesses, DC Electrical conductivity and Sheet resistance of PVDF/GNP coated textiles.

Textile Sample	GNP concentration [%wt.]	T [µm]	$R_{\square}$ [Ω/□]	σ_{eff} [S/m]
T1	13	64	791	19
T2	10	60	804	21

Finally, two different graphene-based coatings loaded with 10% wt. and 13% wt. of GNPs are deposited over the fabric substrate obtaining coated textiles named T1, and T2 respectively. In order to compare PVDF/GNP electrodes with commercial ones, textiles T1 and T2 are shaped identically to the dimensions of commercially available electrodes using Cricut®, a computer controller smart fabric cutter. As reference, two commercial electrodes are selected, i-e., a commercial wearable ECG chest strap, consisting of 2 pairs of rectangular and rounded-rectangular dry electrodes and a disposable Ag/AgCl wet electrode. As a result, the subsequent PVDF/GNP electrodes prepared are shown in Fig. 2(a) and (b). As shown in Table 1, these are designated

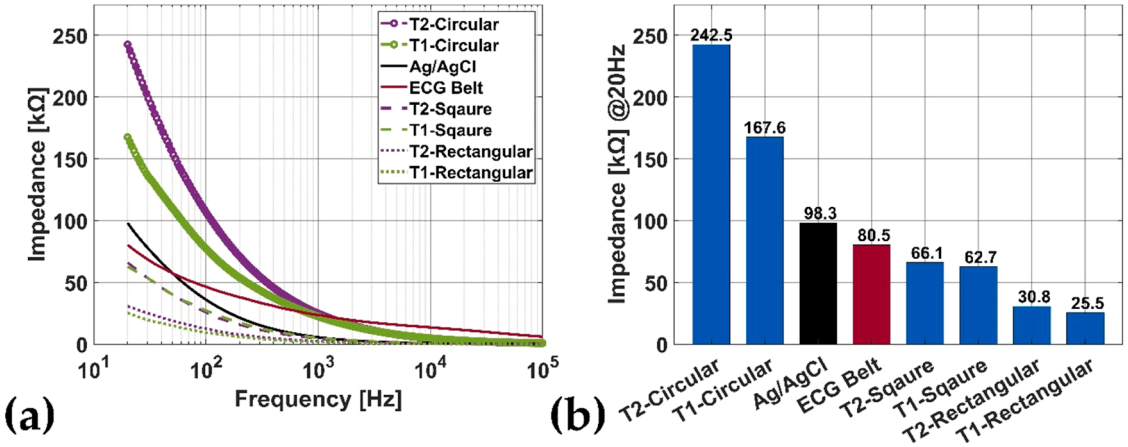

Fig. 7. Skin-electrode impedance spectrum magnitude of the dry electrode of PVDF/GNP electrodes compared to commercial chest belt ranging from 20 Hz to 100 kHz (b) skin-electrode impedance at 20 Hz for each electrode.

Table 3
Electrode RC equivalent model parameters from impedance measurements.

Electrodes Types	RC equivalent model parameters		
	R_p (kΩ)	C_p (nF)	R_s (Ω)
Ag/AgCl	72.00	29.90	328
ECG Belt	36.70	10.00	8890
T1-Rectangular	15.70	101.00	170
T2- Rectangular	18.20	71.60	188
T1-Square	37.70	31.60	324
T2-Square	37.70	36.70	300
T1-Circular	63.20	5.58	879
T2-Circular	95.90	6.05	883

here as T*x*-Square, T*x*-Rectangular, and, T*x*-Circular with *x* equal to 1 or 2 depending on the employed textile sample (T1 or T2) and active contact area of 15.71 cm^2, 5.75 cm^2, and 4.52 cm^2 respectively. For each PVDF/GNP electrode, an extra space of 5 mm width on the top and bottom is included, besides the active skin-contact area, as a contact pad for electrical connections.

To attach electrical wires to the electrodes, the contact pad of the PVDF/GNP electrode is coated with air-drying silver paint Taab Electrodag 915. After coating, the sample is left in the open air for 30 mins to dry out the paint. Later, a wire is attached to the silver-painted contact pad using CircuitWorks conductive epoxy CW2460 and cured in the oven at 60 °C for 60 min to ensure a strong mechanical bond along with good electrical conductivity. Table 1 also reports the contact area of the PVDF/GNP electrodes.

2.2. Morphological, chemical, and physical characterization

The morphology of PVDF/GNP coatings is analyzed using a Zeiss Auriga high-resolution SEM available at the Sapienza Nanotechnology and Nanoscience Laboratory (SNN-Lab) of Sapienza University of Rome. The composite samples are fractured in liquid nitrogen and coated with ~20 nm-Cr using a Quorumtech Q150T sputter coater, in order to prevent charging.

Then, in order to assess the crystal structure of PVDF, X-ray power diffraction (XRPD) analysis is performed and XRPD data are collected with a Bruker AXS D8 Advance equipment operating in θ/θ geometry in transmission mode. The instrument is fitted with incident beam focusing Göbel mirrors and a PSD VÅntec-1D. PVDF/GNP coatings are gently ground in an agate mortar to produce a powder that is loaded in a 0.7 mm diameter SiO_2-glass capillary. Then, capillaries are mounted on standard goniometer heads and aligned along the beam-path. The angular range 2θ is set from 5° up to 90°, being 0.022° the 2θ step size and 2 s the counting time. The aim is to verify the presence of β-phase in the PVDF/GNP composite since this composite structure is associated with improved electrical and mechanical [33].

Finally, hydrophobicity is assessed through the measurement of water contact angles (CAs). Such measurements are carried out by using

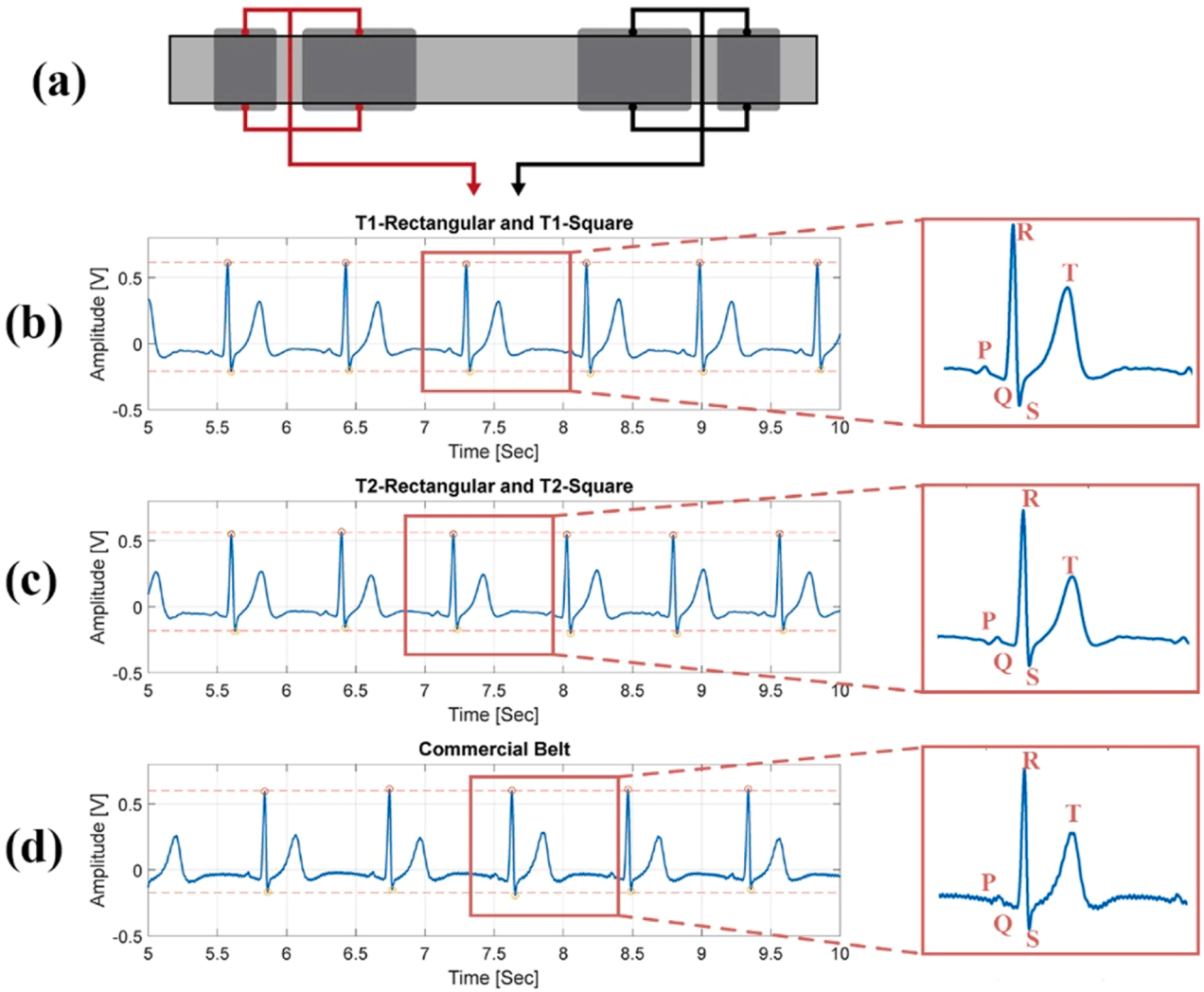

Fig. 8. Comparison of ECG signal of PVDF/GNP electrodes to the commercial ECG belt and identification of the ECG signal features in each case.

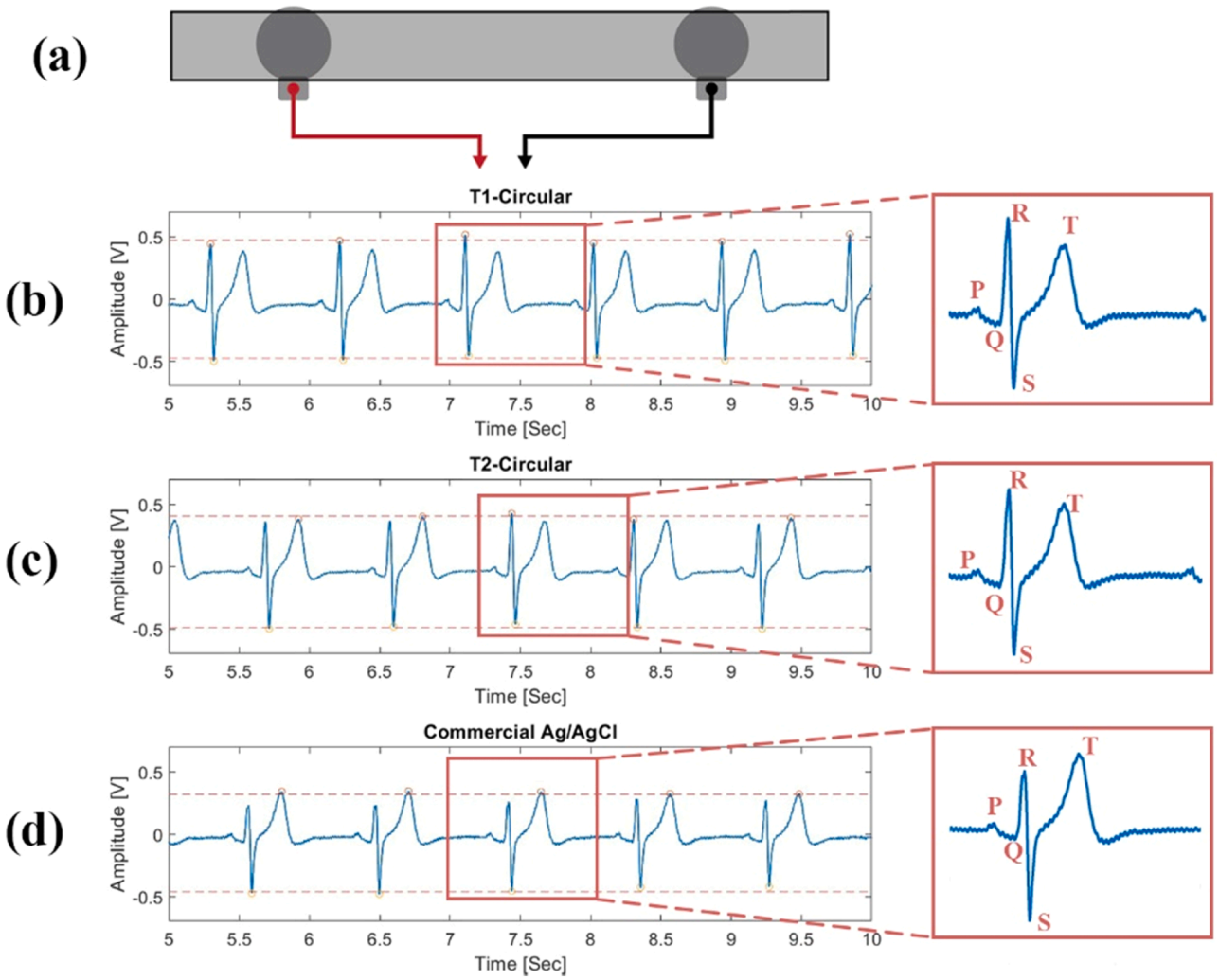

Fig. 9. Comparison of ECG signal of PVDF/GNP electrodes to the commercial Ag/AgCl electrodes and identification of the ECG signal features in each case.

an optical CA meter available at SNN-Lab and casting ~2 μl water droplets on the coating surface.

2.3. Electrical characterization

2.3.1. DC electrical characterization

The electrical characterization is performed by first measuring the sheet resistance $R_{\square}$ of the produced square-shaped samples before reshaping them as the desired electrodes. To avoid errors introduced by the additional resistance of the leads and clips, a four-wire (Kelvin) probe method is preferred [34]. This type of measurement requires a separate programmable current source (ammeter) and a voltmeter.

As shown in Fig. 3, the sample is sourced with current using Keithley 6221 AC/DC generator and the resultant voltage drop is recorded using a Keithley 2182 nano-voltmeter, while both instruments are managed by a Keithley USB to GPIB adaptor and custom-designed software interface in LabVIEW.

Finally, the electrical conductivity σ for each sample is estimated as:

$$\sigma = \frac{1}{R_{\square}\, t} \tag{1}$$

where t is the sample thickness.

2.3.2. Skin-electrode impedance

Each electrode, dry or wet, set up a unique electrolyte-electrode interface with the skin based on its surface morphology. This contact is characterized as skin-electrode impedance and plays an important role in measuring biopotential signal quality since lower skin-electrode impedance eventually results a better signal quality [16]. The skin-electrode interface can be modeled mathematically as an equivalent RC circuit model [8,35–37]. Wet electrodes and dry electrodes, due to their different surface contact mechanism, establish a completely different interface with the skin. A wet electrode can be characterized as a typical electrode-electrolyte interface using a half-cell voltage and parallel RC equivalent element for gel and epidermis (stratum corneum) as shown in Fig. 4(a), whereas, in a dry electrode the skin-electrode contact is not uniform due to the absence of conductive gel and the presence of air or sweat between electrode and skin, so rather it can be characterized as a sum of multiple parallel RC equivalent elements as shown in Fig. 4(b). The overall electrical behavior of the skin-electrode can be simplified to a first-order RC time constant model [35] (Fig. 4(c)) consisting of a series resistance *Rs* and a parallel RC element with resistance *Rp* and capacitance *Cp*. Consequently, the skin-electrode impedance in frequency domain of each electrode can be written as:

$$Z_{ELE}(j\omega) = R_s + \frac{R_p}{1 + j\omega R_p C_p} \tag{2}$$

where ω is the angular frequency and j is the imaginary unit.

The values of parameters *Rp* and *Cp* are specified by ANSI/AAMI and ENI standards. They are equal to 0.62 MΩ and 4.7 nF respectively. Then,

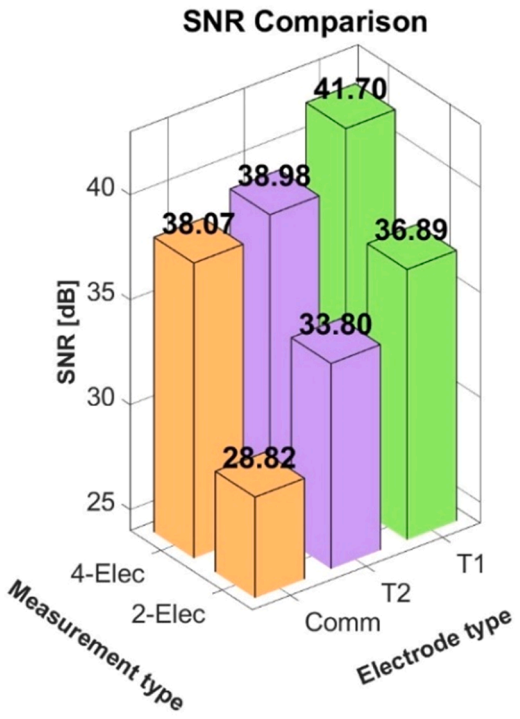

Fig. 10. Comparison of electrodes types and measurement setup based on SNR.

the skin-electrode impedance along with the electrode impedance shall not attenuate the signal more than 20% of the specified value [38,39].

Several different skin-electrode contact methods are used in [40–43] all employing one, two, or three electrodes in contact with the skin. In the following, the skin-electrode impedance measurement is performed by using two electrodes placed on the inner forearm 5 cm apart from each other as depicted in Fig. 4(d). Elastic Velcro straps are used to hold firmly the electrodes in contact with the skin. Keysight E4980AL Precision LCR meter with a four-wire probe is used to record the impedance spectrum within the frequency range from 20 Hz to 100 kHz. Each measurement is taken after placing the electrodes on the skin for 3 min to properly rest the electrode and avoid any variation in the measurement.

Since in this measurement two electrodes are used, the overall impedance magnitude $Z_{Total}(j\omega)$ comprises the impedance of the first electrode $Z_{ELE1}(j\omega)$, the body $Z_{body}(j\omega)$, and the second electrode $Z_{ELE2}(j\omega)$ as shown in Fig. 4(e). It can be expressed as:

$$|Z_{Total}(j\omega)| = \left|2 \times Z_{ELE}(j\omega) + Z_{body}(j\omega)\right| \tag{3}$$

Considering the body impedance can be neglected compared to the electrode impedance, the $Z_{Total}(j\omega)$ can be expressed as:

$$|Z_{Total}(j\omega)| \approx \left|2 \times Z_{ELE}(j\omega)\right| \tag{4}$$

2.3.3. ECG electrode measurement

Generally, a heart is represented by a dipole [44], and during cardiac depolarization, the electrical activity of the heart can be monitored by placing two or more electrodes on several different anatomical spots on

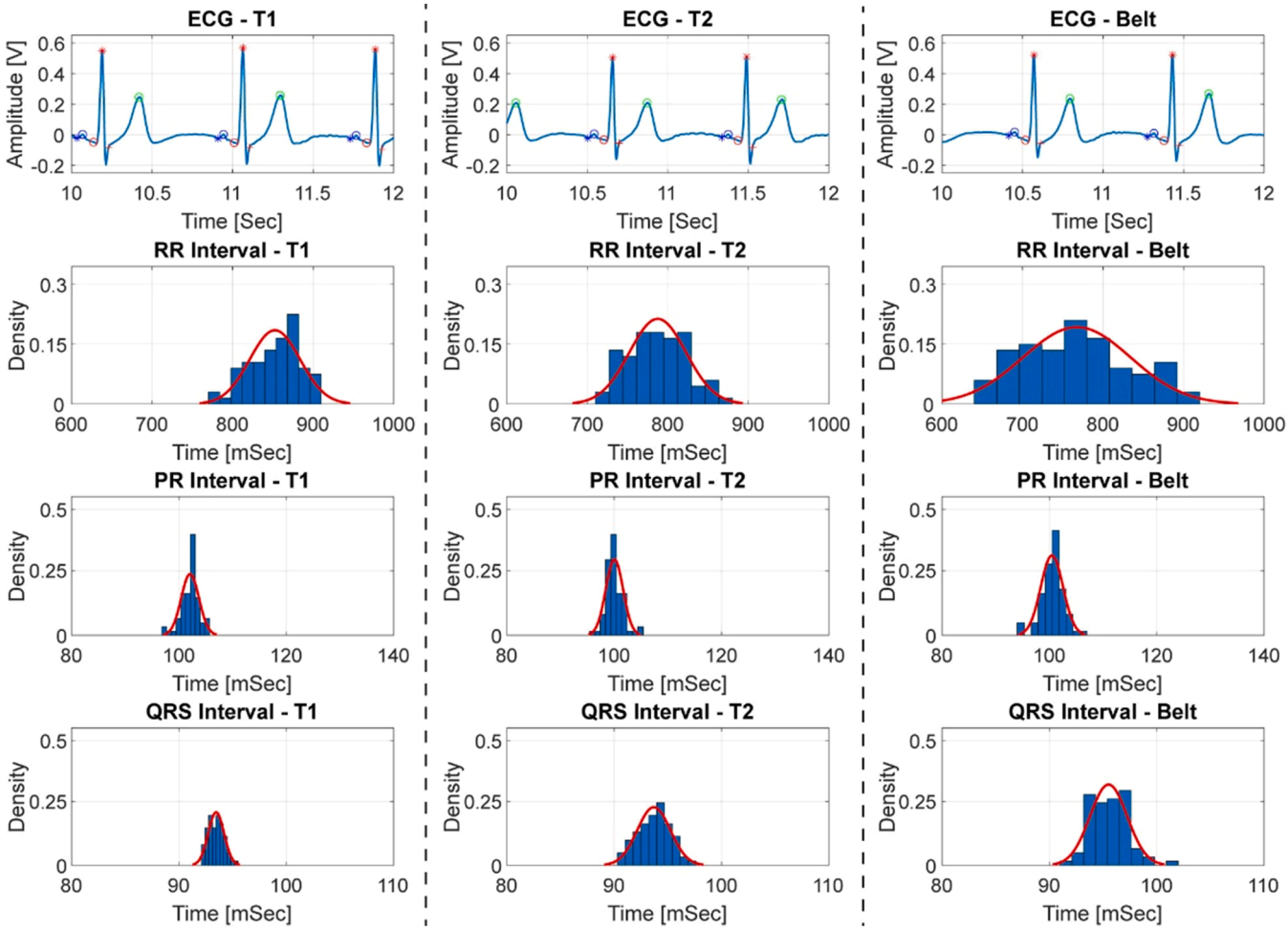

Fig. 11. Histogram and distribution fit of RR, PR, and QRS interval of 60-*sec* measurement of 4-electrode measurements.

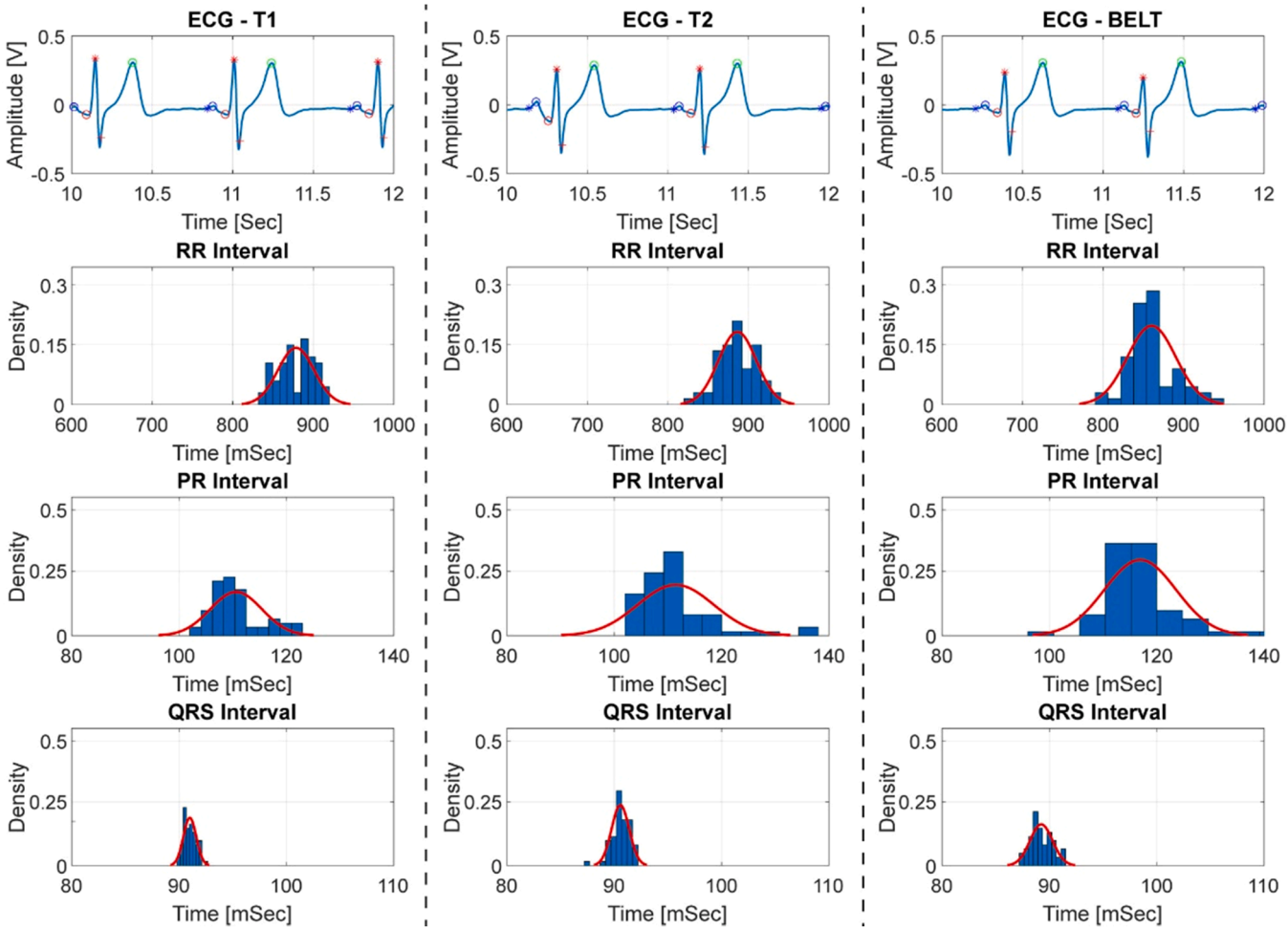

Fig. 12. Histogram and distribution fit of RR, PR, and QRS interval of 60-*sec* measurement of 2-electrode measurements.

the patient's body (most commonly the chest or wrists). In this regard, the produced graphene-based textile electrodes are used to monitor the ECG signals of a healthy patient and the obtained data are compared with the ECG measurement taken using commercial electrodes.

As shown in Fig. 5(a), the ECG measurement setup consists of Stanford Research Systems Low noise preamplifier MODEL SR560. This device has two major cons, that is, (i) it incorporates a differential signal amplification mode with a gain set here at 500, as well as (ii) signal filtration using a bandpass filter set here at a lower and upper cutoff frequency of 0.03 Hz and 30 Hz respectively. The output signal of the pre-amplifier is digitized at 10 kSPS by a multifunction National Instrument NI-USB-6001 data acquisition system interfaced with NI-DAQmx LabView.

Hence, a single-lead ECG measurement is obtained with one or more pairs of electrodes attached to an elastic belt, and the belt is wrapped around the chest of the test subject to hold the electrodes underneath firmly. A 3 M Red Dot electrode is placed under the chest as ground. The measurements are taken at room temperature without preparing the skin i.e. without applying gel or other conductive substances or water drops. Each measurement is taken for one minute on the same subject and the electrode's position on the body was kept identical to achieve comparable results. Since the ECG measurements are non-identical to different subjects and environmental conditions, all the measurements are taken on the same day and on the same subject along with keeping the conditions consistent.

The ECG signal features and morphology play an important role in the assessment of asymmetries in heart activity, which leads to the diagnosis of different heart-related diseases. A normal ECG rhythm is divided into different segments for better distinction, i-e P, Q, R, S, T, and U, as shown in Fig. 5(b), reporting a typical ECG signal rhythm of a healthy heart. Therefore, clear identification of each segment in the ECG signal measurement is necessary. The P-wave is generated due to atrial depolarization and the duration is in the range of ~100 ms. The depolarization of the ventricles causes the QRS-interval and its duration is normally less than ~100 ms. The T-wave represents the repolarization of ventricles and it is round in shape. Finally, the U-wave follows the T-wave and, in some cases, is not recorded so its absence is acceptable [45].

To investigate the effect of the contact area and the GNP concentration variation, several measurements are recorded and their characteristics are compared based on two suitable figures of merit. (i) The SNR, defined as the ratio between the signal peak and noise standard deviation, and (ii) the Vp-p, defined as the maximum amplitude of the acquired signal.

3. Results and discussion

3.1. Morphology

The crystal structure of GNPs, PVDF, and PVDF/GNP coatings are studied through XRPD analysis and the results are reported in Fig. 6(a) considering a diffraction angle 2θ ranging between 20° and 50° It is noticed that GNPs have one crystal peak at $2\theta = 26.6°$ while the principal crystalline peaks of neat PVDF films are observed for $2\theta = 17.76°$, 18.42°, 20.00°, 25.69°, 26.68° and they correspond to α-phase peaks [46]. Then, comparing the crystalline peaks of neat PVDF and of

PVDF/GNP coatings filled with 9% wt. of GNPs, it appears that α-phase PVDF crystal peaks change when GNPs are added in the PVDF polymer matrix. In fact, the intensity peaks related to α-phase sharply reduce or became broad. Moreover, the α-phase peak at $2\theta = 17.76^\circ$ almost disappears, and the critical α-phase crystal peak is shifted from $2\theta = 20^\circ$ to $2\theta = 20.7^\circ$ and converts wide broad peak. All these changes indicate the transformation from α-phase into β-phase due to the nucleation effect of GNPs on polymer crystal phases, improving coating electrical properties [46]. Furthermore, the presence of GNPs in PVDF/GNP coatings is evident from the peak at $2\theta = 26.8^\circ$, indicating the GNP crystal structure.

The SEM images of a graphene based sensor is depicted in Fig. 6(b). At first, the image clearly depicts the coated and uncoated portions of the textile. Then, it is evident that the graphene coating is uniformly distributed on the surface of the selected commercial fabrics and GNPs are uniformly and homogeneously distributed.

Finally, the wettability properties of the uncoated and of the PVDF/GNP coated fabrics are assessed through the measurement of the contact angle (CA). In particular, the CA measurements are performed during the water droplet release and after 30 min, on both the uncoated and coated fabrics. As shown in Fig. 6(c) the CAs on the uncoated fabric is equal to $93^\circ \pm 3^\circ$ and decreases up to $51^\circ \pm 3^\circ$ after 30 min. On the other hand, the CA of coated fabric increases noticeably, reaching values as high as $159^\circ \pm 3^\circ$ during water droplet release and remain quite constant over time, being equal to $153^\circ \pm 3^\circ$ after 30 min. Thus, we conclude that uncoated fabric is hydrophilic while the graphene coated fabric is hydrophobic and its hydrophobicity does not change over time. Furthermore, the enhanced hydrophobic and antimicrobial characteristics of graphene-coated electrodes could be beneficial in sustaining their efficiency over longer durations without compromising their response [5].

3.2. Electrical characterization

Research in the past has shown that graphene based polymer coatings are highly electrically conductive [31] and therefore tend to be suitable to be used as biopotential electrodes. The produced samples T1 and T2 are electrically characterized using the experimental setup described in Section 2.3.1 by evaluating their sheet resistance $R_{\square}$ and extracting their effective electrical conductivity σ by means of Eq. (1) and the results are reported in Table 2.

As expected, the GNP filler concentration significantly affects the DC electrical conductivity of the fabric-coated samples. Consequently, a higher concentration of GNPs filler leads to higher conductivity, that is, it increases from 18 S/m to 21 S/m for 10% wt. and 13% wt., respectively.

3.3. Skin electrode impedance

Skin-electrode impedance measurements are made utilizing the experimental setup described in Section 2.3.2.

The electrode impedance spectrum (EIS) results are shown in Fig. 7 (a) taken from PVDF/GNP coated electrodes with different GNP concentrations and sizes identified in Table 1. Considering that the skin-electrode impedance may be affected by the applied pressure from the elastic strap, the pressure is carefully kept homogenous for every measurement.

To authenticate the monotonicity of the achieved results, each measurement is repeated several times on the same day and the mean of those measurements is reported here. It is observed that the behavior of the electrodes is nearly unchanged during those repeated measurements. Moreover, regardless of keeping the electrode attached to the skin for a long period, no irritation or abnormal skin reaction is noted on the surface of the skin beneath the PVDF/GNP electrode.

In all the measurements, the commercial electrodes show higher skin-electrode impedances (98.32 Ω for Ag/AgCl electrodes and 80.48 Ω for commercial chest belt at starting frequency 20 Hz) compared to the GNP dry electrodes except for the T1-Circular and T2-Circular electrodes. The circular electrodes, due to their only concentrated small electrical contact on the bottom establish larger electrical resistance for the current to follow, unlike other electrodes where the electrical contact is spread across a larger area of the electrode. Therefore, the Circular electrodes although have a relatively similar skin contact area to Rectangular electrodes, result in larger skin-electrode impedance.

Moreover, the sample T1-Rectangular indicates the least impedance magnitude of 26 kΩ at 20 Hz, which is 377% less than the Ag/AgCl electrode and 308% less than the commercial chest belt. The impedance magnitude obtained from the samples T2-Rectangular, T1- Square, and T2- Square ar 30.77 Ω, 62.74 Ω, and 66.12 Ω at 20 Hz frequency respectively as shown in Fig. 7(b).

It is noticed from the results that the electrode contact area with the skin significantly influences the skin-electrode impedance. The larger the skin contact area of the electrode, the lower the impedance. Presumably, the skin-electrode impedances from PVDF/GNP electrodes showed significantly lower values at the same frequencies compared to the dry electrodes presented in [15,16], and [17].

In addition, the response of dry electrodes in the presence of skin perspiration is also investigated. For that matter, a NaCl solution is prepared to replicate the effect of sweat. One droplet (precisely 20 μl volume) of the solution is transported on the surface of each dry electrode using a pipette before placing the electrode on the skin. It is observed that the presence of sweat between the skin and the electrode introduces noteworthy improvement in the skin-electrode impedance magnitude. The skin-electrode impedance decreases in the presence of sweat. This means that skin perspiration can be profitable in GNP dry electrodes' performance.

As discussed earlier in Section 2.3.2, the skin-electrode interface is modeled as a simplified first-order RC time constant equivalent circuit. A program for the minimum root-mean-square error method is written to evaluate the estimated model parameters R_s, C_p, and R_p from the electrode impedance measurement results as indicated in Fig. 4(c). The estimated model parameter values for each type of electrode are given in Table 3.

3.4. ECG measurement

The measurements are taken by placing the electrode in two different arrangements, the 2-Electrode method, and the 4-Electrode method, replicating the commercial chest belt arrangement and commercial Ag/AgCl electrode arrangement to achieve comparable results. In the 4-Electrode arrangement, both Rectangular and Squared electrode pairs are attached identical to the belt, whereas, in the 2-Electrode arrangement, the Circular electrodes are attached as shown in Fig. 8(a) and Fig. 9(a) respectively. The measurement results for electrode types T1 and T2 compared to respective commercial electrodes are shown in Fig. 8 and Fig. 9(b), (c), and (d). It is evident from the results that the ECG signal sinus rhythm is similar to the expected shape as illustrated earlier in Fig. 5(b) along with that all vital features of ECG signals are clearly visible in the measurements of the developed electrodes. In addition to that, the ECG signal morphology is much more comprehensible and cleaner compared to respective commercial electrodes.

To evaluate SNR, the following Eq. (4) is applied on a 60 s ECG measurement.

$$SNR = 20log_{10}\left(\frac{V_{pp}}{2\sigma_n}\right) \tag{4}$$

where V_{pp} is taken from the QRS complex amplitude and the σ_n from the segment between T and P where the signal is isoelectric generally.

Fig. 10 shows that the SNR values of all the developed electrodes are higher than the respective commercial electrodes. The sample T1 in the 4-Electrode arrangement exhibits the highest SNR value of 41.7 dB as expected due to the fact that the sample T1 possesses the lowest skin-

electrode impedance which results in a higher peak-to-peak voltage and lower noise in the recorded ECG signal. The samples T2 also show comparable SNR values of 38.98 dB to the commercial belt SNR value of 38.07 in the 4-Electrode method. Furthermore, the T1-Circular and T2-Circular electrodes also show higher SNR, 36.89 and 33.80, compared to Ag/AgCl electrodes, which is 28.82, even though the skin-electrode contact impedance of these electrodes is higher. It is because the fabric-based developed electrodes are much more flexible and adhere better to the skin under the presence of the belt as opposed to Ag/AgCl electrodes, which are attached to the skin by their self-adhesive gel.

ECG signal features and their intervals play an important role in diagnosing cardiac diseases. The RR-interval, PR-interval, and QRS-interval are the most characteristic intervals in clinical practices, for instance, the assessment of PR and QRS intervals provide information about the atrioventricular and ventricular conduction, respectively [47]. To investigate the variation of these crucial ECG intervals, extraction of the ECG signal features is required. In this regard, an open-source signal processing toolkit "BioSigKit" [48] is used in MATLAB.

Identification of ECG signal features and distribution fit of the above-mentioned intervals is summarized in Fig. 11 and Fig. 12 delivering a side-by-side comparison of developed and commercial electrodes. Both the PVDF/GNP electrodes, T1 and T2, show lower distribution spread: around the mean compared to the commercial ECG belt and Ag/AgCl electrodes whereas sample T1 show the least distribution spread among all three cases. The developed electrodes in both cases show lower spread around the mean and hence shall be acceptable for the accurate measurements of RR-interval, PR-interval, and QRS interval analysis.

4. Conclusion

In this work, novel graphene-based wearable dry electrodes for high-quality and continuous biosignal detection are presented. These electrodes are produced by casting conductive GNP nanofillers mixed with PVDF onto a flexible textile substrate. The resulting coated fabrics show very low skin-electrode impedance, which is an important factor in stable and high-quality ECG signal acquisition. The ECG signal measurements are compared with different commercial electrodes and, consequently, the developed electrodes show better SNR and ECG signal morphology. Moreover, the ECG signal feature extraction is performed and it is observed that all essential ECG signal features are clearly identified and the detected RR, PR, and QRS intervals show very small variations over time. Conclusively, the PVDF/GNP coated electrodes perform better than commercially available gelled electrodes and other dry electrodes recently presented in the literature. The quality of the detected ECG signal allows clear identification of the most important ECG signal features making them suitable for the detection of abnormalities in the heart activities.

Declaration of Competing Interest

The authors declare that they have no known competing financial interests or personal relationships that could have appeared to influence the work reported in this paper.

Data availability

Data will be made available on request.

References

[1] Cardiovascular Diseases (CVDs), 2021. https://www.who.int/news-room/fact-sheets/detail/cardiovascular-diseases-(cvds. accessed May. 03, 2023).

[2] Anna Karilainen, Thomas Finnberg, Thorsten Uelzen, Klaus Dembowski, J. Muller, Mobile patient monitoring based on impedance-loaded saw-sensors, IEEE Trans. Ultrason. Ferroelectr. Freq. Control 51 (11) (2004) 1464–1469.

[3] Zhimin Xu, Zuxiang Fang, A clustered real-time remote monitoring system for out-of-hospital cardiac patients, in: 2008 International conference on biomedical engineering and informatics 1, IEEE, 2008, pp. 610–614.

[4] Khairul A. Sidek, Ibrahim Khalil, Herbert F. Jelinek, Ecg biometric with abnormal cardiac conditions in remote monitoring system, IEEE Trans. Syst., Man, Cybernetics 44 (11) (2014) 1498–1509.

[5] Hossein Cheraghi Bidsorkhi, Negin Faramarzi, Babar Ali, Lavanya Rani Ballam, Alessandro Giuseppe D'Aloia, Alessio Tamburrano, Maria Sabrina Sarto, Wearable graphene-based smart face mask for real-time human respiration monitoring, Mater. Des. (2023), 111970.

[6] Babar Ali, Negin Faramarzi, Umar Farooq, Hossein Cheraghi Bidsorkhi, Alessandro Giuseppe D'Aloia, Alessio Tamburrano, Sabrina Sarto Maria, Graphene-based smart insole sensor for pedobarometry and gait analysis, IEEE Sens. Lett. (2023).

[7] Ju-Yeoul Baek, Jin-Hee An, Jong-Min Choi, Kwang-Suk Park, Sang-Hoon Lee, Flexible polymeric dry electrodes for the long-term monitoring of ecg, Sens. Actuators, A 143 (2) (2008) 423–429.

[8] Yu Mike Chi, Tzyy-Ping Jung, Gert Cauwenberghs, Dry-contact and noncontact biopotential electrodes: methodological review, IEEE Rev. Biomed. Eng. 3 (2010) 106–119.

[9] Shiwei Xu, Meng Dai, Canhua Xu, Chaoshuang Chen, Mengxing Tang, Xuetao Shi, Xiuzhen Dong, Performance evaluation of five types of ag/agcl bio-electrodes for cerebral electrical impedance tomography, Ann. Biomed. Eng. 39 (2011) 2059–2067.

[10] Anthony J. Portelli, Slawomir J. Nasuto, Design and development of non-contact bio-potential electrodes for pervasive health monitoring applications, Biosensors 7 (1) (2017) 2.

[11] Andrew Searle, L.J.P.M. Kirkup, A direct comparison of wet, dry and insulating bioelectric recording electrodes, Physiol. Meas. 21 (2) (2000) 271.

[12] Jae-Woong Jeong, Min Ku Kim, Huanyu Cheng, Woon-Hong Yeo, Xian Huang, Yuhao Liu, Yihui Zhang, Yonggang Huang, John A. Rogers, Capacitive epidermal electronics for electrically safe, long-term electrophysiological measurements, Adv. Healthc. Mater. 3 (5) (2014) 642–648.

[13] Seung Min Lee, Jeong Hun Kim, Hang Jin Byeon, Yoon Young Choi, Kwang Suk Park, Sang-Hoon Lee, A capacitive, biocompatible and adhesive electrode for long-term and cap-free monitoring of eeg signals, J. Neural Eng. 10 (3) (2013), 036006.

[14] Anna Gruetzmann, Stefan Hansen, Jörg Müller, Novel dry electrodes for ecg monitoring, Physiol. Meas. 28 (11) (2007) 1375.

[15] Md Abu Zahed, Partha Sarati Das, Pukar Maharjan, Sharat Chandra Barman, Md Sharifuzzaman, Sang Hyuk Yoon, Jae Yeong Park, Flexible and robust dry electrodes based on electroconductive polymer spray-coated 3d porous graphene for long-term electrocardiogram signal monitoring system, Carbon 165 (2020) 26–36.

[16] Amer Abdulmahdi Chlaihawi, Binu Baby Narakathu, Sepehr Emamian, Bradley J. Bazuin, Massood Z. Atashbar, Development of printed and flexible dry ecg electrodes, Sens. Biosensing. Res. 20 (2018) 9–15.

[17] Murat A. Yokus, Jesse S. Jur, Fabric-based wearable dry electrodes for body surface biopotential recording, IEEE Trans. Biomed. Eng. 63 (2) (2015) 423–430.

[18] W.David Hairston, Keith W. Whitaker, Anthony J. Ries, Jean M. Vettel, J. Cortney Bradford, Scott E. Kerick, Kaleb McDowell, Usability of four commercially-oriented eeg systems, J. Neural Eng. 11 (4) (2014), 046018.

[19] Vaidotas Marozas, Andrius Petrenas, Saulius Daukantas, Arunas Lukosevicius, A comparison of conductive textile-based and silver/silver chloride gel electrodes in exercise electrocardiogram recordings, J. Electrocardiol. 44 (2) (2011) 189–194.

[20] Gilsoo Cho, Keesam Jeong, Min Joo Paik, Youngeun Kwun, Moonsoo Sung, Performance evaluation of textile-based electrodes and motion sensors for smart clothing, IEEE Sens. J. 11 (12) (2011) 3183–3193.

[21] Wanqing Wu, Sandeep Pirbhulal, Arun Kumar Sangaiah, Subhas Chandra Mukhopadhyay, Guanglin Li, Optimization of signal quality over comfortability of textile electrodes for ecg monitoring in fog computing based medical applications, Future Generat. Comput. Syst. 86 (2018) 515–526.

[22] Kostya S. Novoselov, Andre K. Geim, Sergei V. Morozov, De-eng Jiang, Yanshui Zhang, Sergey V. Dubonos, Irina V. Grigorieva, Alexandr A. Firsov, Electric field effect in atomically thin carbon films, Science 306 (5696) (2004) 666–669.

[23] Xu Du, Ivan Skachko, Anthony Barker, Eva Y. Andrei, Approaching ballistic transport in suspended graphene, Nat. Nanotechnol. 3 (8) (2008) 491–495.

[24] Alexander A. Balandin, Suchismita Ghosh, Wenzhong Bao, Irene Calizo, Desalegne Teweldebrhan, Feng Miao, Chun Ning Lau, Superior thermal conductivity of single-layer graphene, Nano Lett. 8 (3) (2008) 902–907.

[25] I.W. Frank, David M. Tanenbaum, Arend M.van der Zande, Paul L. McEuen, Mechanical properties of suspended graphene sheets, J. Vacuum Sci. Technol. b 25 (6) (2007) 2558–2561.

[26] Gunho Jo, Minhyeok Choe, Sangchul Lee, Woojin Park, Yung Ho Kahng, Takhee Lee, The application of graphene as electrodes in electrical and optical devices, Nanotechnology 23 (11) (2012), 112001.

[27] Anindya Nag, Arkadeep Mitra, Subhas Chandra Mukhopadhyay, Graphene and its sensor-based applications: a review, Sens. Actuators, A 270 (2018) 177–194.

[28] Sina. Ebnesajjad, Fluoropolymers: properties and structure, Non-Melt Processible Fluoroplastics (2000) 23–32.

[29] Babar Ali, Hossein C. Bidsorkhi, Alessandro G. D'Aloia, Marco Laracca, Maria S. Sarto, Graphene-based flexible dry electrodes for biosignal detection, in: 2022 IEEE international conference on flexible and printable sensors and systems (fleps), IEEE, 2022, pp. 1–4.

[30] Florian Geyer, Maria D'Acunzi, Azadeh Sharifi-Aghili, Alexander Saal, Nan Gao, Anke Kaltbeitzel, Tim-Frederik Sloot, Rüdiger Berger, Hans-Jürgen Butt,

Doris Vollmer, When and how self-cleaning of superhydrophobic surfaces works, Sci. Adv. 6 (3) (2020) eaaw9727.
[31] Hossein C. Bidsorkhi, Lavanya Rani Ballam, Alessandro G. D'Aloia, Alessio Tamburrano, Giovanni De Bellis, Maria Sabrina Sarto, Flexible graphene based polymeric electrodes for low energy applications, in: 2020 IEEE 20th international conference on nanotechnology (IEEE-nano), IEEE, 2020, pp. 263–266.
[32] Fabrizio Marra, Alessandro Giuseppe D'Aloia, Alessio Tamburrano, Isabel Maria Ochando, Giovanni De Bellis, Gary Ellis, Maria Sabrina Sarto, Electromagnetic and dynamic mechanical properties of epoxy and vinylester-based composites filled with graphene nanoplatelets, Polymers (Basel) 8 (8) (2016) 272.
[33] Cheraghi Bidsorkhi, Hossein, Alessandro Giuseppe D'Aloia, Alessio Tamburrano, Giovanni De Bellis, Maria Sabrina Sarto, Waterproof graphene-pvdf wearable strain sensors for movement detection in smart gloves, Sensors 21 (16) (2021) 5277.
[34] "ASTM F390 - 11 Standard test method for sheet resistance of thin metallic films with a collinear four-probe array (Withdrawn 2020)." https://www.astm.org/Standards/F390.htm (accessed Oct. 07, 2021).
[35] Roman Kusche, Steffen Kaufmann, Martin Ryschka, Dry electrodes for bioimpedance measurements—Design, characterization and comparison, Biomed. Phys. Eng. Express 5 (1) (2018), 015001.
[36] Valerio De Santis, Valeiy Martynyuk, Alessandro Lampasi, Mykola Fedula, Manuel Duarte Ortigueira, Fractional-order circuit models of the human body impedance for compliance tests against contact currents, AEU-Int. J. Electron. Commun. 78 (2017) 238–244.
[37] Valerio De Santis, Pierre A. Beeckman, Domenico Alessandro Lampasi, Mauro Feliziani, Assessment of human body impedance for safety requirements against contact currents for frequencies up to 110MHz, IEEE Trans. Biomed. Eng. 58 (2) (2010) 390–396.
[38] "ANSI/AAMI EC11:1991/(R)2001 - Diagnostic electrocardiographic devices, 2ed." https://webstore.ansi.org/standards/aami/ansiaamiec1119912001 (accessed Oct. 14, 2021).
[39] "AAMI/IEC-60601-2-47 | Medical electrical equipment - Part 2-47: particular requirements for the basic safety and essential performance of ambulatory electrocardiographic systems (ANSI/AAMI/IEC 60601-2-47:2012) | document center, Inc." https://www.document-center.com/standards/show/AAMI/IEC-60601-2-47 (accessed Oct. 14, 2021).
[40] Bahareh Taji, Adrian DC Chan, Shervin Shirmohammadi, Effect of pressure on skin-electrode impedance in wearable biomedical measurement devices, IEEE Trans. Instrum. Meas. 67 (8) (2018) 1900–1912.
[41] Wei Zhou, Wei Liu, Shaoyu Liu, Chenying Zhang, Zhijia Shen, Guobiao Zhang, Characterization of impedance properties of metal dry bioelectrodes with surface microstructure arrays, Sens. Actuators, A 263 (2017) 252–258.
[42] Sajjad Asadi, Zijun He, Fatemeh Heydari, Dan Li, Mehmet Rasit Yuce, Tuncay Alan, Graphene elastomer electrodes for medical sensing applications: combining high sensitivity, low noise and excellent skin compatibility to enable continuous medical monitoring, IEEE Sens. J. 21 (13) (2020) 13967–13975.
[43] Anas. Albulbul, Evaluating major electrode types for idle biological signal measurements for modern medical technology, Bioengineering 3 (3) (2016) 20.
[44] John H. Holt Jr, Anthony Cl Barnard, M. Stuart Lynn, Peder Svendsen, A study of the human heart as a multiple dipole electrical source: I. Normal adult male subjects, Circulation 40 (5) (1969) 687–696.
[45] A.B. de Luna, Textbook of clinical electrocardiography. Textbook of clinical electrocardiography, 1987, https://doi.org/10.1007/978-94-009-4299-8.
[46] Hossein Cheraghi Bidsorkhi, Alessandro Giuseppe D'Aloia, Giovanni De Bellis, Alessandro Proietti, Andrea Rinaldi, Marco Fortunato, Paolo Ballirano, Maria Paola Bracciale, Maria Laura Santarelli, Maria Sabrina Sarto, Nucleation effect of unmodified graphene nanoplatelets on pvdf/gnp film composites, Mater. Today Commun. 11 (2017) 163–173.
[47] Adel Nada, Gary A. Gintant, Robert Kleiman, David E. Gutstein, Christer Gottfridsson, Eric L. Michelson, Colette Strnadova, et al., The evaluation and management of drug effects on cardiac conduction (pr and qrs intervals) in clinical development, Am. Heart J. 165 (4) (2013) 489–500.
[48] H. Sedghamiz, Biosigkit: a matlab toolbox and interface for analysis of biosignals, J. Open Source Software 3 (30) (2018) 671, https://doi.org/10.21105/JOSS.00671. Oct.